PCCP

Accepted Manuscript

ROYAL SOCIETY OF CHEMISTRY

www.rsc.org/pccp

PCCP

Dynamic Article Links ►

Cite this: DOI: 10.1039/c0xx00000x

www.rsc.org/xxxxxx

ARTICLE TYPE

Aqueous production of oxygen atoms from hydroxyl radicals

Edelsys Codorniu-Hernández,[1] Kyle Wm. Hall,[1,2] Daniel Ziemianowicz,[1] Sheelagh Carpendale,[2] Peter G. Kusalik[1]*

Received (in XXX, XXX) Xth XXXXXXXXX 20XX, Accepted Xth XXXXXXXXX 20XX
DOI: 10.1039/b000000x

The behavior of the hydroxyl radical (OH*) in solution is significant to a broad range of scientific and technological fields. OH* is considered a highly reactive, short-lived species and previous studies have neglected the possibility of encounters of two OH* in solution. However, these encounters may be nonnegligible in environments with elevated local OH* concentrations, such as under many *in vivo* processes and within nuclear infrastructure. High concentrations of OH* in vivo are considered to be very dangerous; OH* has been related to many ailments ranging from cancer to Alzheimer's disease. Here we probe details of the reactions and interactions that can occur between two OH* in water by utilizing Car-Parrinello molecular dynamics simulations and advanced visualization techniques. The recombination reaction to form hydrogen peroxide is confirmed for the singlet electronic state. In contrast, the triplet state yields an oxygen atom, O(aq). This species has been previously detected in experimental water-radiolysis studies, but its origin could not be determined. O(aq) is a much more potent biradical than its parent OH* and its presence can impact many *in vivo* processes. This study also reveals that the hemibonded interaction plays key role in the behavior of OH*(aq). Our findings have major implications to the scientific understanding of the impacts of high local OH* concentrations, such during oxidative stress and in aging processes. Given its importance, this study will form the basis of further experimental and theoretical investigations exploring the role of O(aq) in a number of contexts.

Introduction

The hydroxyl radical has been a key species in a diverse range of areas such as the origins of life, cosmic and nuclear reactions, atmospheric chemistry, and the biomolecular mechanisms of fatal diseases such as cancer.[1-5] OH* is a highly reactive species owing to the presence of an unpaired electron within its electronic structure. It has been identified as the strongest and most dangerous reactive oxygen species (ROS), being called the "atmospheric vacuum cleaner" because of its ability to remove important pollutants from the air.[5] The OH*, along with the superoxide anion and hydrogen peroxide, are involved in the redox-dependent regulation of different cellular functions including energy metabolism and responses to stress or growth signals.[4] As a ROS, OH* is constantly produced and eliminated *in vivo* as part of normal biochemical functions.[6]

The lifetime of OH* is typically very short because of its reactive nature, and its concentration is expected to be low. However, there is growing evidence of the overproduction of this radical in certain environments, such as production via radiolysis within nuclear infrastructure,[1] and under some important *in vivo* processes (i.e. under oxidative stress,[6] as part of auto-immune responses,[7] and under oxidative-damage cellular death,[8] exploited by some classes of antibiotics to kill bacteria). High concentrations of OH* *in vivo* are considered to be very dangerous because, unlike other ROS, OH* cannot be eliminated by enzymatic reactions. Despite the negative impacts of increased concentrations of OH* in cancer cells, it has been suggested that ROS might function as a "double-edge sword"; they can induce and maintain the oncogenic phenotype of cancer cells, but can also function as anti-tumorigenic species.[2] Consequently, there are ongoing studies exploiting this biochemical feature to develop therapeutic strategies to kill cancer cells preferentially through ROS-mediated mechanisms.[2,6,9] To advance both knowledge and utilization of this potent radical, it is crucial to understand the possible reactions of OH* radicals in solution.

The behaviour of OH* radicals in solution has been the focus of several experimental[10,11] and theoretical investigations,[12-20] despite the challenges associated with studying this short-lived species. We have recently reported results on the solvation, mobility, and reactions of OH* in an aqueous environment (water and ice) utilizing Car-Parrinello molecular dynamics simulations.[13,17,21] We have also validated the reliability of the applied methodology, in an extensive benchmarking study with high level *ab-initio* calculations[19] (see Computational Details section). This previous work provided clear and consistent evidence of the ability of the OH* to form hemibonds with water molecules, as an alternative interaction when the formation of hydrogen bonds is impeded. However, the rather fundamental question of what happens when two

PCCP

Dynamic Article Links ►

Cite this: DOI: 10.1039/c0xx00000x

www.rsc.org/xxxxxx

ARTICLE TYPE

hydroxyl radicals approach each other in water remains virtually unexplored, experimentally or theoretically. The dissociation of hydrogen peroxide is a possible source of a OH* pair in solution.[22] Furthermore, hydrogen peroxide has been recently identified as the signal molecule of aging,[4] and is produced by mitochondria to control cellular growth and death; as such, there is a potential source of a OH* pair in cells. Recent findings have shown that the generation of OH* from hydrogen peroxide can occur in the triplet state.[23]Additionally, when two OH* approach each other, as might occur when the local concentration is high (e.g. during radiolysis), there will be significant probability for either singlet state or triplet state encounters. The present study probes the possible outcomes of such encounters.

Computational Details

The Car-Parrinello[24] DFT-based *ab initio* molecular dynamics method was used with the CPMD[25] code to study 62·H_2O-2OH* systems at 310 K in a cubic and periodic simulation box. The local spin density approximation (LSDA) was used to account for the unpaired electron on the OH*. The HCTH/120[26] density functional was employed and the valence-core interactions were described by Troullier-Martins[27] norm-conserving pseudopotentials. In previous reports, we have characterized the solvation and mobility of OH* in water and ice, utilizing the same methodology described herein, including comparisons with the BLYP DFT functional.[13,17,21] Although very similar results were obtained with both functionals, HCTH/120 showed more superior results; BLYP tended to provide an overstructured system compared with experimental studies.[17] More recently we have published a benchmarking study comparing the HCTH/120 functional with high level (MP2, basis set limit CCSD(T) and beyond) *ab initio* calculations in the accurate characterization of the hemibonded interaction and its energy relative to other well-defined hydrogen bond interactions.[19] This gas-phase *ab initio* study validates the HCTH/120 functional for describing the possible interactions that OH* can experience in an aqueous environment.[19] In addition, the results of a further benchmarking study of the interaction of two OH* radicals in the gas phase will presented in a forthcoming paper, in which the results obtained with the HCTH/120 DFT functional are compared with those obtained with the CCSD(T) method. The OH*-OH* hemibonding interaction is much more stable with the HCTH/120 functional relative to the results provided by CCSD(T), finding a minimum structure at short O*-O* separations around 2 Å. However, both methods agree in finding the formation of the triplet oxygen atom and a water molecule as the ground state in the gas phase when zero-point energy corrections are included. The possible existence of a multiference character at shorter O*-O* separations is currently under investigation, comparing the results of HCTH/120 with the MRCISD method. Additionally, we will show that the inclusion of a single water molecule in the gas phase converts a system of two OH* radicals to $O(^3P)$ + $2H_2O$ during optimization. This confirms that there is a significant impact of water molecules on the reaction under study. Therefore, as we will discuss in a forthcoming paper, both zero-point energy corrections and solvent effects contribute to the triplet oxygen and water molecule being the ground state for the HCTH/120 functional in agreement with the results of CCSD(T).

The valence electronic wavefunction was described with a plane wave basis with an energy cutoff of 90 Ry (120 Ry being utilized to obtain the electronic data). Fictitious electronic masses of 100 and 400 a.u. were both employed. The fictitious electron kinetic energy and the dynamics of atoms were controlled by a chain of three Nose-Hoover thermostats[28] operating at characteristic frequencies of 6000 cm^{-1} and 2000 cm^{-1}, respectively. During the 7 ps equilibrations and the subsequent 50 ps of simulations, the total energy was monitored, as was the kinetic energy of the fictitious electronic degrees of freedom. The average fictitious kinetic energy was maintained at levels of 0.03 Ha and remained stable during the whole simulation. The time step was set to 0.1 fs.

Constrained MD (CMD) and Metadynamics. CMD simulations[29] were utilized to determine the free energy for the formation of O(aq) in the triplet state, as well as H_2O_2 and oxywater in the singlet state. Due to the different nature of the reactions, different reactions coordinates were selected for every case. For the formation of O(aq) in the triplet state, the distance O*-H* was chosen as a constraint, where H* is the hydrogen atom transferred and O* is the oxygen atom accepting the transfer. To calculate the free energy for the formation of H_2O_2 from a OH* pair in the singlet state, the O*-O* separation was utilized as a constraint. In turn, to evaluate the possible formation of oxywater, an isomer of H_2O_2 in the singlet state, a hydrogen from H_2O_2 was driven to be transferred to form the O-H_2O complex. In all the cases, for each 0.1 Å increment, the average constraint force was measured over a 20 ps trajectory. From such simulations the free energy profile was obtained from a straightforward thermodynamic integration over the chosen coordinate. Lagrangian metadynamics[30] is a powerful method to quantify the free energy barriers, particularly of rare events. In this work metadynamics was successfully used to track the production of O(aq) starting from the OH*-OH* dimer. Details of this approach have been extensively published.[30,31] The chosen set of collective variables consisted of the O*-H*-O* angle and the H*-O* distance. A preliminary unbiased run at 310 K was used to choose the Gaussian widths, ∂s, as a quarter of the fluctuation of the collective variable with the smallest variation. The scaling factors were defined accordingly. In our case a value of 0.15 was utilized. The Gaussian heights were determined by the underlying potential energy surface and an

PCCP

Dynamic Article Links ►

Cite this: DOI: 10.1039/c0xx00000x

www.rsc.org/xxxxxx

ARTICLE TYPE

imposed upper bound of 0.0005 kcal/mol. Biasing potentials were added with a minimum separation of 100 MD steps. The fictitious masses and force constants for both collective variables were set to 0.1 a.u. and 10 a.m.u, respectively. **Visualization Methods.** Fig. 4, Fig. S3 in SI, and the videos were made using in-house programs written in Processing, http://processing.org. The free energy surface profiles were obtained by plotting the points provided by CPMD. The colour gradient, which was used to indicate the angle values, corresponds to only a hue variation with saturation and value being held constant over the gradient. For the contour plot, a value gradient at constant hue and saturation was used to encode the order of the contours. The contour plot was obtained using interpolation, and then rendering all points that were within 0.5% of the spacing between contours, which was set to be 1.0 kcal/mol. For the videos, the electronic surfaces were created by interpolating the voxel data provided by CPMD, and then rendering a small, semi-transparent coloured sphere for any

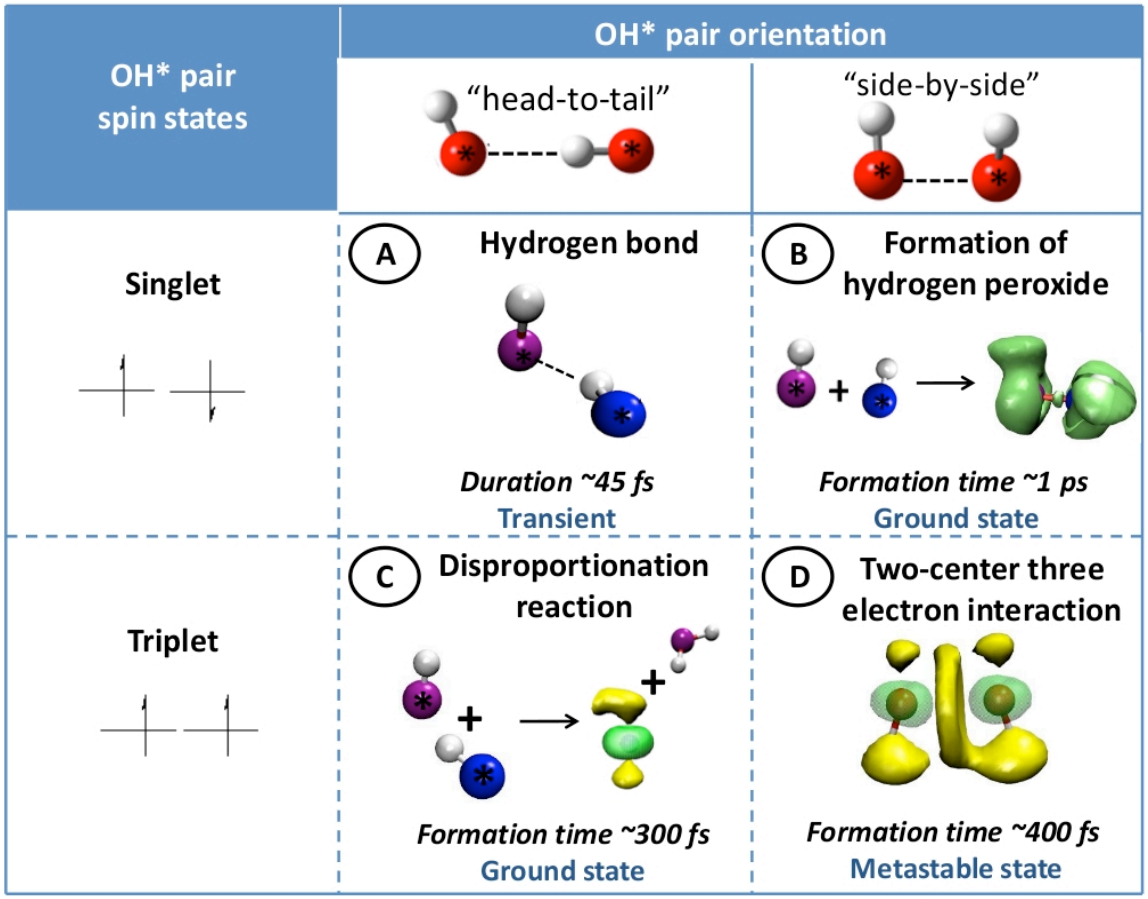

Fig. 1 Schematic diagram showing primary products and key interactions observed when a OH* pair encounter in water. The two possible spin states (singlet and triplet) are considered, and in each case two relative orientations of the OH* pair are distinguished, "head-to-tail" and "side-by-side". In the "head-to-tail" arrangement, the O-H bond of one radical tends to point at the oxygen of the other radical, facilitating the formation of a transient hydrogen bond (A) in the singlet state and the very rapid production of O(aq) in the triplet state (C). The "side by side" arrangement, where the O-H bonds tend to be perpendicular to the r_{OO} vector, is conducive to the formation of hydrogen peroxide in the singlet state (B), and favours a two-center three-electron interaction in the triplet state (D). Electron spin density isosurfaces has been used to highlight the triplet state products, where green and yellow surfaces represent negative (-0.03) and positive spin densities (+0.0004), respectively, for the oxygen atom (C) and the hemibonded interaction (D). The darker green isosurfaces for hydrogen peroxide (B) show the localization of electron pairs (i.e. the ELF).

PCCP

Dynamic Article Links ►

Cite this: DOI: 10.1039/c0xx00000x

www.rsc.org/xxxxxx

ARTICLE TYPE

point that fell within the range of values of interest. This range corresponded to 3.75*10-4 to 4.25*10-4 for the positive spin density, and -0.0335 to -0.0265 for the negative spin density. Atoms within 2.50 Å of either hydroxyl radical's oxygen appear in the video with opacity increasing from completely transparent at 2.50 Å separation to completely opaque at 0.96 Å. Each atom has a tail corresponding to its recent positions in the local frame of reference of the videos, where the z axis of the coordinate system is aligned with the vector between the oxygen atoms of the two hydroxyl radicals. The electronic surfaces lack such tails and only the instantaneous surfaces are rendered for a given iteration of the simulation. Chemical bonds were drawn in the videos when the separation between two atoms was less than 1.152 Å with the bonds transitioning from completely transparent at 1.152 Å to completely opaque at 0.96 Å. The videos are shown in perspective with a $\pi/4$ shear, which spreads the depth of the videos horizontally. All of the above information applies to the still images of the system in Fig. 4 except that the cut-off for drawing chemical bonds was set to 1.056 Å and there are no atomic tails. Additional details regarding the visualizations herein presented will be provided in a future article.

Results and Discussion

Primary products and key interactions

Fig. 1 summarizes our observations from extensive Car-Parrinello molecular dynamics simulations of a OH* pair in water in both possible electronic spin states, singlet and triplet. These results reveal that the relative orientation of the two radicals in combination with their spin state dictates the observed products obtained in water. Henceforth, the hydrogen and oxygen atoms of these radicals are denoted as H* and O*, respectively. At O*-O* separations of roughly 3 Å, a hydrogen bonding interaction is found to be dominant for the singlet and triplet states. In the singlet state, a hydrogen bonded radical pair is found to be transient (see Fig. 1A), transitioning rapidly to a "side-by-side" orientation with shorter O*-O* separations and yielding hydrogen peroxide as expected (see Fig. 1B). Hydrogen peroxide can be expected, given sufficient time, to eventually decompose into water and (molecular) oxygen. In the triplet state, hydrogen bonding forces tend to align the approaching hydroxyl radicals in a "head-to-tail" configuration. This is the thermodynamically favored configuration of two OH* in the gas phase, based on high level *ab initio* calculations,[32] and is leads to a disproportionation reaction. In our aqueous phase simulations this arrangement is conducive to rapid H-atom transfer, which produces a very reactive triplet oxygen atom and a water molecule on a time scale of ~300 fs (see Fig. 1C and Video1_O(aq)_production in the SI). This disproportionation reaction is considerably faster than the expected spin relaxation of the radical pair which is estimated to be between 0.1 and 1 ns.[33] Taken together with evidence that the dissociation of hydrogen peroxide to form a OH* pair can occur in the triplet state,[23] it is reasonable to expect that there is opportunity for the formation of O(aq) under appropriate experimental conditions.

In the gas phase, this disproportionation reaction has been demonstrated [32,34,35] to be the most energetically favored, and gas phase experimental data at 300 K have indicated either a zero or a very small barrier (1 kcal/mol) for O(g) production in the triplet state.[36] Oxygen atoms had been suggested as a primary species in irradiated water[37,38] as well as the precursors of the O_2 generated in γ-ray irradiated $FeSO_4$-$CuSO_4$ solutions.[39] The presence of triplet state O(aq) has been detected experimentally during water radiolysis studies;[40,41] unfortunately, the origin of O(aq) could not be experimentally determined, nor have there been theoretical studies probing the behavior in condensed phase previously reported. The possible production of this potent oxidant has enormous implications, especially in life science applications. It is notable that the disproportionation reaction in the singlet state, leading to the products H_2O and a singlet oxygen atom, $O(^1D)$ (aq), appears to be an unfavorable pathway in aqueous solution, in accord with previous gas phase calculations.[34] In addition, we have observed that a OH* pair in the triplet state can, with apparently lower probability, associate with a different relative geometry, as shown in Fig. 1D. In such an arrangement the O*-O* distance is less than 2.5 Å with no hydrogen atom between the two oxygens; each unpaired electron appears to be involved in a two-center three-electron interaction, known alternatively as a "hemibond" or as a 2c-3e bond.[42] Hemibonding interactions between OH* and water[18,19] or halide anions[20] have been characterized previously. In the past, 2c-3e bonds were considered an artifact of the DFT methods.[16] However, recent benchmark studies utilizing both DFT and high-level *ab initio* approaches have demonstrated the formation and stability of $X\cdots OH_2$ (X=OH*, F, Cl, Br)[18,19,20,43-45] and Y···NH3 (Y=F, Cl)[42,45-47]hemibonded complexes. Our current data indicates that the hemibond is also an accessible structure for two OH*. As illustrated by the electron spin density isosurfaces in Fig 1D (also see Video_3_OH*-dimer in SI) the unpaired electrons delocalize on the four atoms of this persistent structure. The O*-O* distance of this configuration has an average value of 2.1 Å, and exhibits an oscillatory behaviour resembling bond stretching vibrations for heavy atoms experiencing a relatively weak interaction (see Fig. S2 in SI). A very similar arrangement with an O-O separation of about 2.0 Å has been recently reported in two high level gas phase *ab initio* studies,[32,35] one of them[32]

PCCP

Dynamic Article Links ►

Cite this: DOI: 10.1039/c0xx00000x

www.rsc.org/xxxxxx

ARTICLE TYPE

labeling this geometry as the cis-H_2O_2 molecule in the triplet state.

Free energy profiles for singlet state reactions

As stated above, the expected recombination reaction of two hydroxyl radicals in the singlet state to produce hydrogen peroxide in water is confirmed in our study. This reaction has been well studied experimentally[49-52] in the condensed phase, where it is important in the generation of corrosive hydrogen peroxide and oxygen molecules in water-cooled nuclear power plants. In a more recent study,[49] pulse radiolysis of N_2O-saturated water combined with UV transient absorption detection allowed the determination of the rate constant for this reaction from 150 to 350 ºC. This study also reported the aqueous OH* absorption spectrum between 230 and 320 nm up to 350 ºC. The bands in this spectrum were finally assigned after considerable debate by Chipman[53] utilizing the results of high level *ab initio* calculations. Chipman[53] showed that the main experimental aqueous absorption band peak at ~230 nm arises from OH*-H_2O hemi-bonded structures. Although the formation of hydrogen peroxide is expected from the recombination of a singlet state OH* pair in water, a comprehensive molecular level understanding of the reaction mechanism and its free energy profile are crucial to further investigations on the applications of the OH* in solution. In Fig. 2, the relative free energies of key structures that appear as the separation between the two radicals is reduced are presented. "Head-to-tail" arrangements, which are about 25 kcal/mol less stable than the final product, are observed at larger separations. As the separation is reduced below 2.6 Å, "side-by-side"configurations (reminiscent of the hemibonded arrangement in triplet state) become more stable, and lead to the formation of hydrogen peroxide as the O*-O* distance is further decreased. The formation of hydrogen peroxide from two hydroxyl radicals in the singlet state is an effectively barrier-less reaction, whereas the reverse reaction is about 25 kcal/mol uphill. Without doubt, hydrogen peroxide will be the major product for the singlet state system. Electronic details for this reaction (isosurfaces showing evolution of the HOMO and HOMO-1, and ELF), as well as radial distribution functions and coordination numbers showing the solvation of hydrogen peroxide in water are provided in SI.

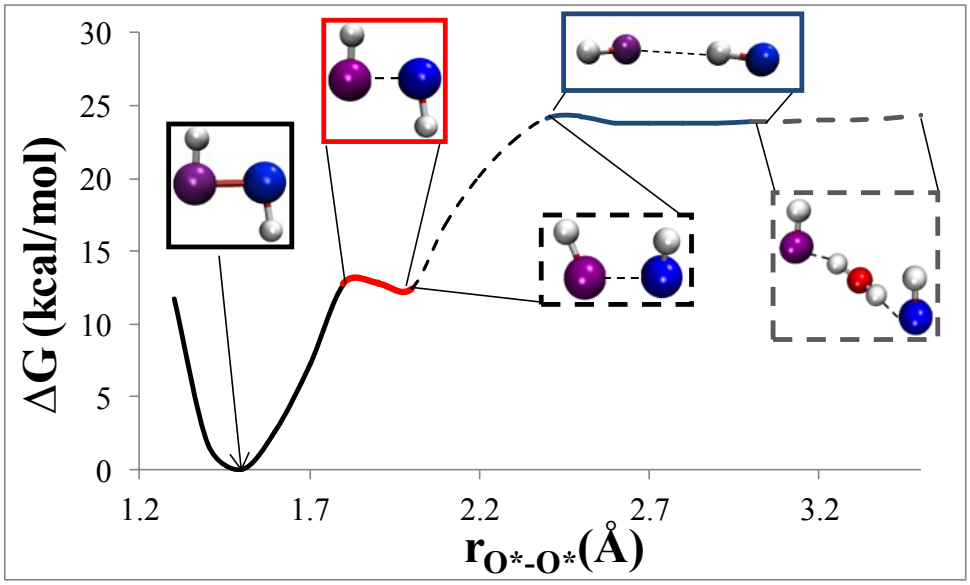

Fig. 2 Free energy (ΔG) profiles at 310 K for the formation of H_2O_2 from two OH*, were the O*-O* distance was utilized as a constraint. The relative free energies for the configuration in which a water molecule bridges the two hydroxyl radicals is shown as a gray dashed line, a blue solid line represents values of "head-to-tail" configurations, and "side-by-side" configurations are shown as a black dashed line (-cis) and a red solid line (-trans); in each case representative configurations are provided as insets. The free energy values corresponding to the global minimum, hydrogen peroxide, are shown with a black solid line. Details on the constrained molecular dynamics simulations used to determine these results can be found in the Computational Details section. In the determination of values for ΔG, contributions from the pV term were assumed to be negligible.

PCCP

Dynamic Article Links ►

Cite this: DOI: 10.1039/c0xx00000x

www.rsc.org/xxxxxx

ARTICLE TYPE

In the last decade there has been an ongoing discussion, based on gas-phase theoretical studies, around claims that oxywater (an isomer of hydrogen peroxide, the H_2O-O complex in the singlet state, with an O-O distance of about 1.45 Å) should be a detectable species in experiments.[54] Oxywater did not appear spontaneously as a configuration in our simulations. However, starting from hydrogen peroxide we have forced the system to form oxywater (see Fig. 3); this yields a free energy barrier of about 29 kcal/mol, and confirms that we would not expect oxywater to be observed in (aqueous solution) experiments.

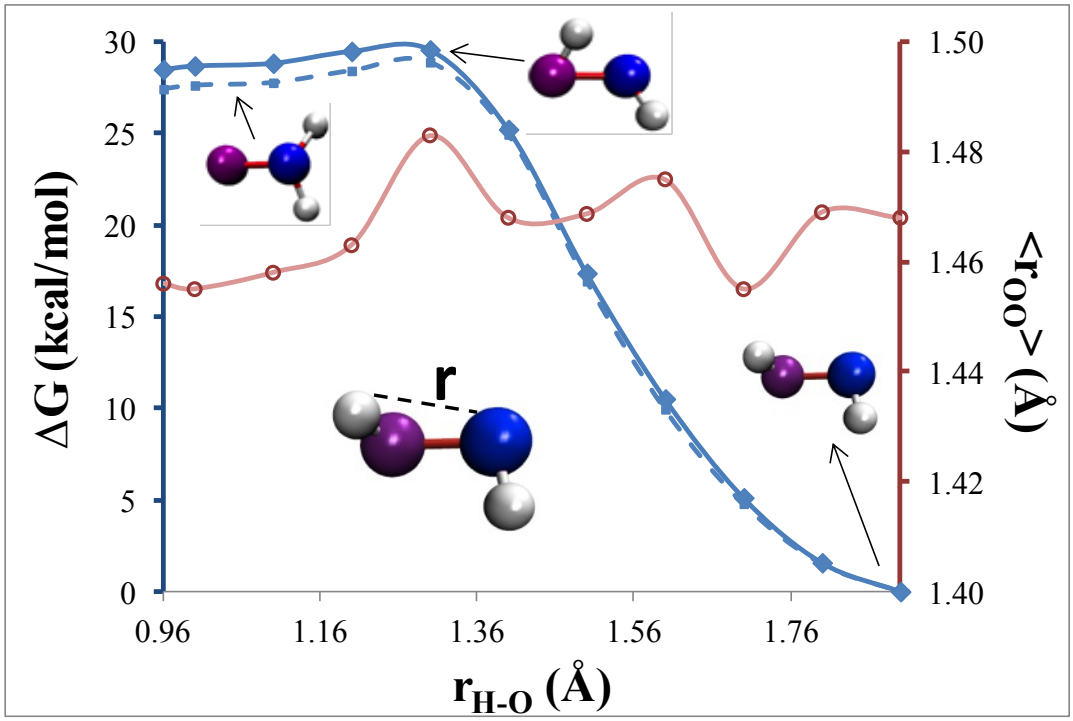

Fig. 3 Free energy (ΔG) profiles at 310 K for the formation of oxywater (O-OH_2 complex) from H_2O_2 in the singlet state. The H-O distance (see inset) was utilized as a constraint. The free energy values (blue y-axis) during the conversion of hydrogen peroxide to the oxywater complex are shown, where the three configurations (hydrogen peroxide, transition state, and oxywater complex) are shown as insets. Results for both forward and backward conversions are provided as solid and dashed lines, respectively. The average r_{OO} (Å) distance is given as a secondary red y-axis, and demonstrates only minor change during the conversion. Details on the constrained molecular dynamics simulations used to determine these results can be found in the Computational Details section. In the determination of values for ΔG, contributions from the pV term were assumed to be negligible.

RAMT plots: tracking geometrical features during the reaction

As stated above, in investigations of the OH* in water the formation of secondary oxidants is always a concern. Hydrogen peroxide is a well known side product from the OH* recombination reaction in the singlet state. However, in our simulations the oxygen atom, O(aq), was very rapidly produced from two OH*(aq) in the triplet state. The H_2O-O triplet state complex observed in the gas phase,[35,54] was not detected in the aqueous environment. Instead, O(aq) appeared to be a weakly hydrated species, with non-persistent interactions with water molecules (see Video2_triplet_O for the solvation of O(aq) in the SI).To explore further the geometric details associated with the formation of the oxygen atom in water, a set of radially-

PCCP

Dynamic Article Links ►

Cite this: DOI: 10.1039/c0xx00000x

www.rsc.org/xxxxxx

ARTICLE TYPE

angularly mapped trajectory (RAMT) plots were generated from each simulation trajectory (see description in SI). From the RAMT plots presented in Fig. 4 and Fig. S3 in SI, we can deduce the time evolution of general geometrical features for all

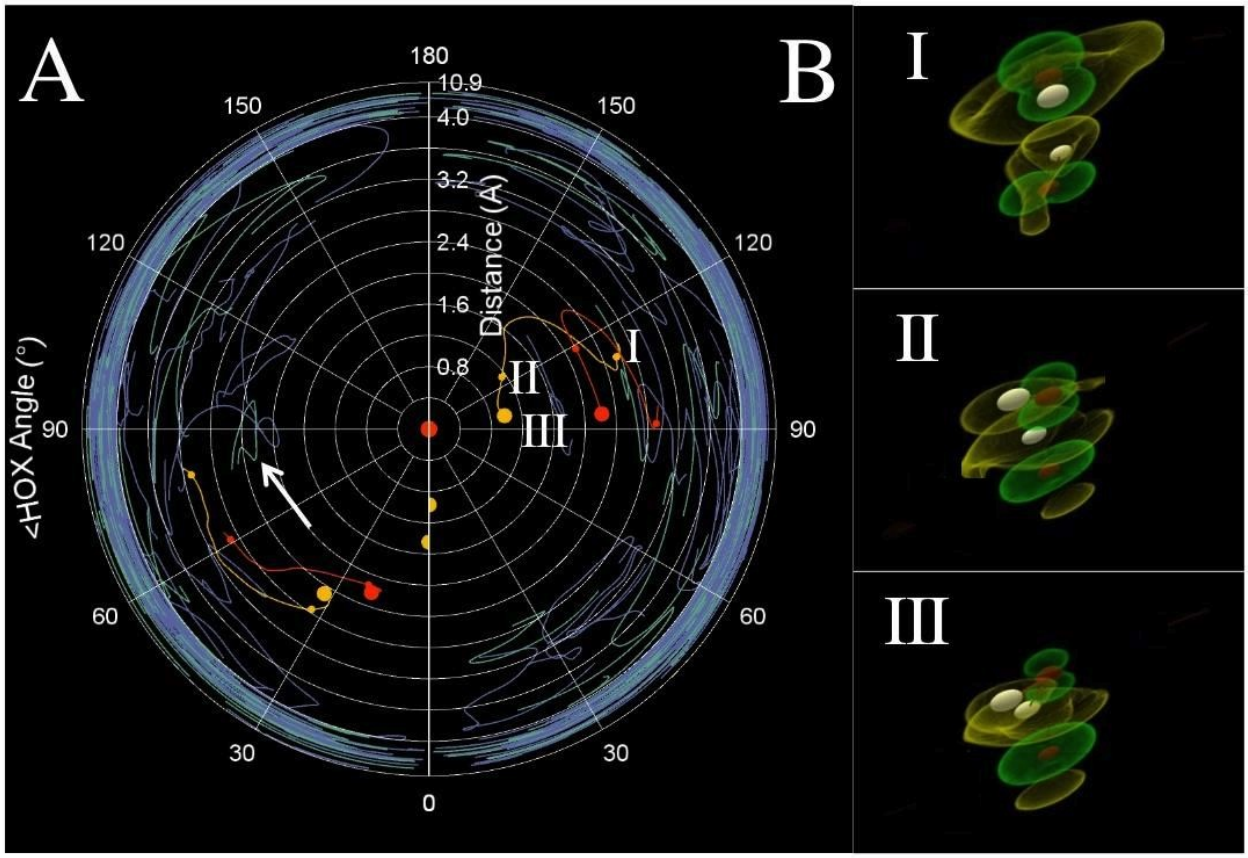

Fig. 4 Radially-angularly mapped trajectory (RAMT) plot of a representative system trajectory where the 2OH*(aq) → O (aq) + H_2O (l) reaction occurs. To understand the RAMT plot for a given OH*, imagine placing the radical's oxygen atom at the origin of the OH* frame of reference, and aligning the O-H bond (the radical's C∞ symmetry axis) with the zenith direction. Plotting atomic trajectories in this (r, θ)-space shows the time evolution of the system from the perspective of the radical. The yellow, red, green and blue traces correspond to the projected trajectory traces of the OH* hydrogen, the OH* oxygen, the H_2O oxygen atoms and the H_2O hydrogen atoms, respectively, up to 10 fs after the transition state of the reaction. Sides A and B correspond to the RAMT plots for the OH* that becomes the triplet oxygen atom and for the OH* that becomes the water molecule, respectively. The two semi-circular RAMT plots are divided by a white vertical line, where the final positions of the OH* atoms that define the frame of reference are shown as semi-circles along the line. The large dots in each RAMT plot indicate the final positions of the atoms of the other radical within the frame of reference of the central OH*. A white arrow in side A identifies an oxygen atom participating in a hemibonding interaction. Key states during the reaction are labelled as I, II, and III in the RAMT plot (with corresponding dots), while the corresponding configurations (showing only the two OH* radicals converting into an O(aq) and H_2O and including electron spin densities) are shown as insets. The distance scale has two linear regions, from 0.0 Å to 4.0 Å and from 4.0 Å to 10.9 Å. Additional details are provided in the Computational Details section and in the SI.

PCCP

Dynamic Article Links ►

Cite this: DOI: 10.1039/c0xx00000x

www.rsc.org/xxxxxx

ARTICLE TYPE

the reactions. We see from Fig. 4B, i.e. the trajectory as viewed by the OH* that accepts the hydrogen atom, that initially the OH* pair is in a "side-by-side" configuration and has an O*-O* separation of about 3 Å (see I on RAMT plot). The radicals then evolve to a "head-to-tail" configuration as the system approaches the transition state, which corresponds to II in Fig. 4B. During this evolution, the H*O*H* angle varies in the range 110° to 140°. The hydrogen atom transfer is nearing completion at III with an angle close to the HOH bond angle for a water molecule. The O*-O* separation changes from about 3 Å at I to about 2 Å at II and III, while the separation of the H-atom being transferred changes from about 2.57 Å at I to 1.15 Å at II, reaching a value of 0.98 Å at III as the new water molecule forms. The insets I, II and III at the right of the figure show the geometries and delocalization of the spin densities corresponding to the "initial", "transition", and "post-transition" states, respectively, where the post-transition state is roughly 10 fs after the transition state. As the system approaches the transition state, the spin density delocalizes among cell all the atoms involved, and exhibits more "O-atom like" features on the atom donating the hydrogen atom. Even 100 fs after the transition state, the spin density remains delocalized among all the atoms and the O*-O* separation is still relatively small.

Switching our attention to the trajectory as viewed by the OH* that loses the H-atom (Fig. 4A), it is notable that the OH* that accepts the H-atom (to form a water molecule) can be seen to be adopting a "head-to-tail" configuration as the transfer proceeds. As we shall detail in a forthcoming article, all the observed reactions proceed through a hemibonded-assisted mechanism. More specifically, a neighboring water molecule is always found to engage in a hemibonded interaction with the radical pair as the system approaches the transition state; the white arrow in Fig. 4A indicates the trajectory of the water oxygen forming the hemibond. It is notable that the hemibonded interaction converts to a transient H-bond once the O(aq) atom forms.

Free energies for the formation of O(aq)

To help understand the factors influencing the very rapid formation of O(aq), a free energy profile for this process was determined through constrained MD simulations (see details in the Computational Details section) utilizing the O*-H* separation as the constraint coordinate, where H* is the hydrogen atom being transferred and O* is the oxygen atom accepting the hydrogen. The results presented in Fig. 5A confirm that O(aq) is the ground state configuration for the triplet state. A barrier-less reaction was obtained for the formation of O(aq) (VII) from the OH* pair (IV) in the triplet state (through the transient arrangement VI), while the reverse reaction has a barrier of around 10 kcal/mol (see Fig. 5A). The dashed line in this figure represents a local minimum structure obtained for values of the O*-H* separation from 1.7 to 2.3 Å. A typical configuration is represented as (V), in which the two OH* radicals have an O*-O* average distance of 2.1 Å. As stated above, this triplet state OH* dimer is stabilized by a two-center three-electron interaction or "hemibond". As an apparent consequence of this stabilization the spontaneous conversion from this species to O(aq) and H_2O was not observed in our simulations. More information about this dimer has been provided in the SI. A very recent gas phase study reports a similar structure for the cis- triplet hydrogen peroxide.[32]

As presented in Fig. 5A the OH* dimer is less stable than O(aq) and H_2O by about 3 kcal/mol. To explore further details on the shape of the free energy surface governing transitions between the OH* dimer (V) to O(aq) (VII) in the triplet state we have used metadynamics. Fig. 5B shows the free energy landscape as a function of both the O*H separation (r_B) and the O*H*O* angle, where H* is the hydrogen atom being transferred, obtained from metadynamics simulations. This figure indicates that O(aq) is about 1-2 kcal/mol more stable, once again confirming that O(aq) is the global minimum configuration for this state. A barrier of about 2 kcal/mol separates the two arrangements. The two additional basins (VIII and IX) that appear in this free energy surface are not of interest to this study because they occur at larger oxygen-hydrogen separations and correspond to different hydrated forms of O(aq). The key structures identified in Fig. 5 are consistent with those seen in very recent high level *ab initio* calculations.[35] Yet, it is apparent from the present study that solvent effects are playing a significant role favouring the formation of O(aq), as there is no barrier for the reaction observed nor does the O(aq)-H_2O complex persist in our simulations (see Section 1 in SI).

PCCP

Dynamic Article Links ►

Cite this: DOI: 10.1039/c0xx00000x

www.rsc.org/xxxxxx

ARTICLE TYPE

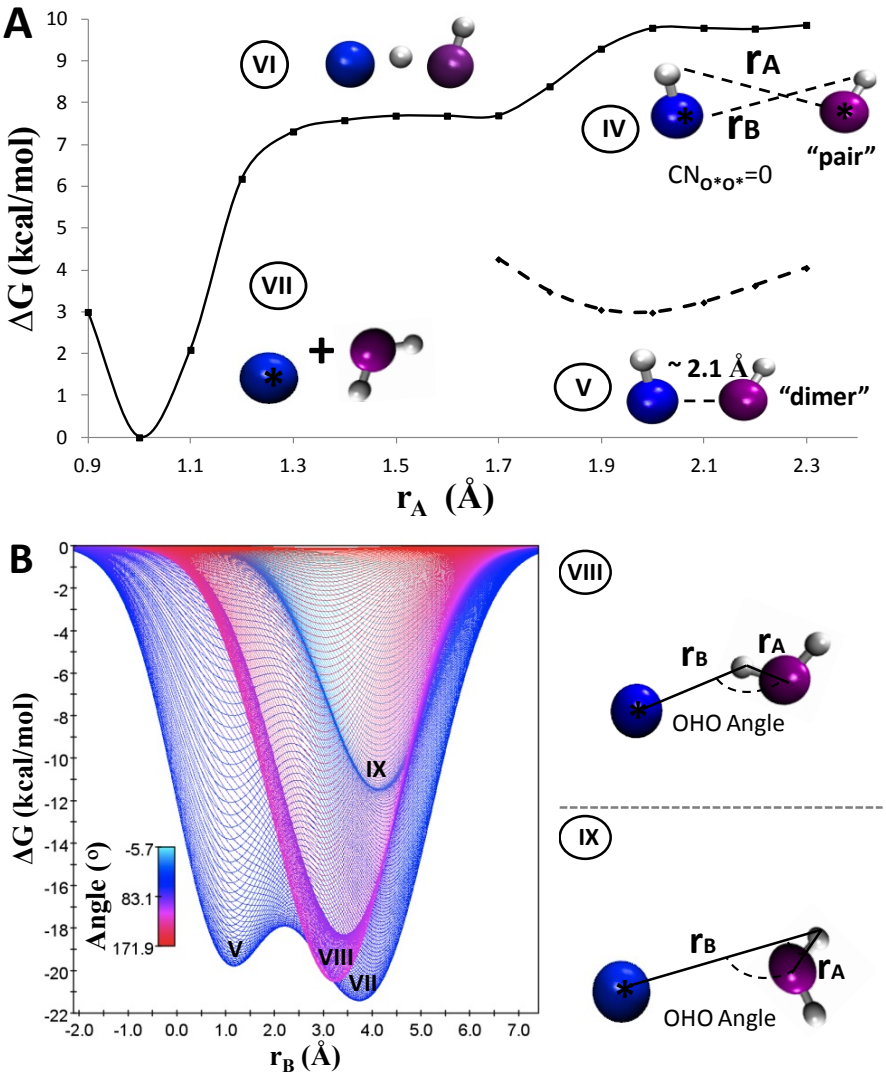

Fig. 5 Free energy (ΔG) profiles at 310 K for different arrangements of the OH* pair in the triplet state. Frame A shows data from constrained molecular dynamics simulations (see details in the Computational Details section), where the displacement coordinate "r_A" represents the distance between the transferred hydrogen atom and the oxygen atom accepting the hydrogen (see inset). The primary species observed, IV: the radical pair, V: the radical dimer, VI: transient state and VII: O(aq) and water, are shown as insets. To achieve the separated pair of radicals (r_A=1.7 to 2.4 Å), the two oxygen atoms were constrained to have a separation > 2.5 Å, as otherwise an OH* dimer configuration (V) resulted. The results in Frame B were obtained from metadynamics simulations (see details in the Computational Details section), utilizing the distance between the transferred hydrogen atom and the oxygen atom donating the hydrogen and the <O*H*O* angle (see inset) as collective variables. In the determination of values for ΔG, contributions from the pV terms were assumed to be negligible.

PCCP

Dynamic Article Links ►

Cite this: DOI: 10.1039/c0xx00000x

www.rsc.org/xxxxxx

ARTICLE TYPE

Conclusions

Car-Parrinello molecular dynamics simulations of a OH* pair in aqueous solutions, combined with free energy calculations and advanced visualization techniques were used to provide details of the possible reactions that can occur when two OH* encounter each other in aqueous environments. The relative orientations of the radicals and their spin states favor the formation of different products. The formation of hydrogen peroxide is confirmed in the singlet state, while formation of oxywater is not observed. In the triplet state, O(aq) is produced through a very fast barrier-less reaction. The implications for the formation of the very potent biradical triplet oxygen atom under relatively high local concentrations of OH* in water provides an explanation for the observation of atomic oxygen during water radiolysis experiments[40,41] and may be crucial to understanding several key in vivo phenomenologies, e.g. the free-radical or oxidative-stress hypothesis for aging. Furthermore, O(aq) is expected to have numerous and broad implications as a more potent reactive oxygen species in a variety of contexts, ranging from nuclear reactors to the understanding and controlling of important fatal illnesses such as cancer. This potent oxidant is expected to be valuable in bioanalytical (fingerprinting) techniques for the investigation of critical problems in molecular biology. There are currently ongoing investigations aimed at generating aqueous-soluble precursors of O(aq) to be used as a unique oxidant in life science applications.[55] Therefore, the details on the production of O(aq) provided here are of fundamental importance and are key to both advancing and developing many further investigations across a wide range of fields.

Acknowledgements

We are grateful for the financial support of the Natural Sciences and Engineering Research Council of Canada, the Alberta Innovates - Technology Futures, and the Canadian Foundation for Innovation. We also acknowledge computational resources made available via WestGrid (www.westgrid.ca) and the University of Calgary. E.C-H. thanks Dr. A. Daniel Boese for useful discussions.

References

1. B. C. Garrett, *et al*. *Chem. Rev*., 2005, **105**, 355-3900.
2. D. Trachootham, J. Alexandre, P. Huang, *Nat. Rev. Drug. Disc.,* 2009, **8**, 579-591.
3. M. Valko, C. J. Rhodes, J. Moncol, M. Izakovic, M. Mazur, *Chem. Biol. Interact.,* 2006, **160**, 1-40.
4. M. Giorgio, M. Trinei, E. Migliaccio, P. G. Pelicci, *Nat. Rev. Mol. Cell Bio.,* 2007, **8**, 722-728.
5. I. S. A Isaksen, S. B Dalsøren, *Science*, 2011, **33**, 38-39.
6. H. Pelicano, D. Carney, P. Huang, *Drug. Resist. Updat., 2004,* **7**, 97-110.
7. Y. Yang, A. V. Bazhin, J. Werner, S. Karakhanova, *Int. Rev. Immunol., 2013,* **32**, 249-270.
8. M. A. Kohanski, D. J Dwyer, J. J Collins, *Nat. Rev. Microbiol.,* 2010, **8**, 423-435 .
9. M. López-Lázaro, *Cancer Lett.,* 2007, **252**, 1-8.
10. L-M Dorfman, G- E Adams, Reactivity of hydroxyl radicals in aqueous solution. National Standard Reference Data. U. S. Department of Commerce. 1973.
11. G. V. Buxton, C. L. Greenstock, W. P. Helman, A. B. Ross. *Phys. Chem. Ref. Data,* 1988, **17**: 513-886.
12. A. Galano, M. Narciso-López, M. Fransisco-Marquez, *J. Phys. Chem. A,* 2010, **114**, 5796-5809.
13. E. Codorniu-Hernández, P. G Kusalik, *J. Am. Chem. Soc.,* 2012, **134**, 532-538.
14. P. Vassilev, M. J. Louwerse, E. J Baerends, *J. Phys. Chem. B,* 2005, **109,** 23605-23610.
15. J. M. Khalack, A. P. Lyubartsev. *J. Phys. Chem. A,* 2005, **109**, 378-386.
16. J VandeVondele, M Sprik (2005) A molecular dynamics study of the hydroxyl radical in solution applying self-interaction corrected density functional methods. *Phys Chem Chem Phys* 7: 1363.
17. E. Codorniu-Hernández, P. G Kusalik, *J. Chem. Theory Comput.,* 2011, **7**, 3725-3732.
18. D. M. J Chipman, *Phys. Chem. A,* 2011, **115,** 1161.
19. E. Codorniu-Hernández, A. D Boese, P. G Kusalik. *Can. J. Chem.*, 2013, 91, 544-551.
20. M. Yamaguchi, *J. Phys. Chem. A,* 2011, **115**, 14620-8.
21. E. Codorniu-Hernandez, P. G Kusalik. *Phys. Chem. Chem. Phys.,* 2012, **14**, 11639 -11650.
22. S. Toyokuni, K. Okamoto, J. Yodoi, H. Hiai, *FEBS Lett.,* 1995, *3*58, 1-3.
23. B. Bhattacharjeea, R. Dasa *Molecular Physics: An international Journal at the interface between chemistry and physics,* 2007, **105**, 1053-1057.
24. R. Car, M. Parrinello. *Phys. Rev. Lett.,* 1985, **55**, 2471-2474.
25. CPMD, Copyright IBM Corp. 1990–2006, Copyright MPI für Festkörperforshung, Stuttgart (1997–2001).
26. A. D Boese, N. L. Doltsinis, N. C. Handy, M. Sprik, *J. Chem. Phys.,* 2000, **112**, 1670-1678.
27. N. Troullier, J.L. Martins, *Phys. Rev. B,* 2000, **43**, 1993-2006.
28. G. J. Martyna, M. L Klein, M. Tuckerman. *J. Chem. Phys.,* 1992, **97,** 2635.
29. M. Sprik, G. Ciccotti, *J. Chem. Phys.,* 1998, 109, 7737-7745.
30. A. Laio, M. Parrinello, *Proc. Natl. Acad. Sci. USA,* 2002, **99**, 12562-12566.

PCCP

Dynamic Article Links ►

Cite this: DOI: 10.1039/c0xx00000x

www.rsc.org/xxxxxx

ARTICLE TYPE

31. D. Ensing, A. Laio, M. Parrinello, M. L. Klein. J. Phys. Chem. B, 2005, **109**, 6676-6687.
32. J. G. Hill, G. Bucher. J. Phys. Chem. A, 2014, 118, 2332-2343.
33. B. Brocklehurst, *J. Chem. Soc. Faraday Trans.,* 1979, **75**, 123-140.
34. Y. Ge, K. Olsen, R. I. Kaiser, J. D. Head, *AIP Conf. Proc.,* 2006, **855**, 253-259.
35. J. Li, H. Guo, *J. Chem. Phys.,* 2013, 138, 194304.
36. J-A. Kerr, S-J. Moss (1981) *CRC Handbook of Biomolecular and Termolecular Gas Reactions*, Volume II, CRC Press, Inc. Boca Ratón, Florida., ISBN 0-8493-0376-1.
37. A-O. Allen, *Radiat. Res. Suppl.,* 1964, 4, 54.
38. M. Anbar, Water and aqueous solutions. In Fundamental Processes in Radiation Chemistry (P. Ausloos, Ed.), 1968, Chapter 10, p. 651. Interscience Publishers, New York.
39. E. Bjergbakke, E. J. Hart, *Radiat. Res.* 1971, **45**, 261.
40. W. G Brown, E. J. Hart, *Radiat. Res.,* 1972, **51**, 249-253.
41. W. G. Brown, E. J Hart, M. C. Jr. Sauer, *Radiat Res.,* 1978, **76**, 533-539.
42. I. Fourré, B. Silvi, *Het. Chem.,* 2007, **18**, 135-160.
43. J. Li, Y. Li, H. Guo, *J Chem Phys.,* 2013, **138**, 141102.
44. G. Li, L. Zhou, Q. S. Li, Y. Xie, H. F. III Schaefer *Phys. Chem. Chem. Phys.,* 2012, **14**, 10891.
45. J. Li, R. Dawes, H. Guo, *J. Chem. Phys.,* 2012, **137**, 094304.
46. J. A. Kłos, G. Chałasiński, M. M. Szczęśniak, H. J. Werner, *J. Chem. Phys.,* 2001, **115**, 3085.
47. M. L. McKee, A. Nicolaides, L. A. Radom, *J. Am. Chem. Soc.,* 1996, **118**, 10571.
48. Y. Gao, I. M. Alecu, P. C. Hsieh, B. P. Morgan, P. Marshall, L. N. Krasnoperov. *J. Phys. Chem. A,* 2006, **110 21**, 6844.
49. I. Janik, D. M. Bartels, C. D. Jonah. *J. Phys. Chem. A*, 2007, **111**, 1835-1843.
50. A. J. Elliot. Rate constants and G-values for the simulation of the radiolysis of light water over the range 0-300 ºC. *AECL report* **11073**, 1994.
51. H. Christensen, K. Sehested. *Radiat. Phys. Chem.*, 1981, **18**, 723.
52. A. J. Elliot. *Radiat. Phys. Chem.*, 1989, **34**, 753. A. J. Elliot, D. R. McCracken, G. V. Buxton, N. D. Wood. *J. Chem. Soc., Faraday Trans.* 1990, **86**, 1539.
53. D. M. Chipman. *J. Phys. Chem. A.*, 2008, 112, 13372-13381.
54. P. G. Sennikov, S. K. Ignatov, O. Schrems. *Chem. Phys. Chem.,* 2005, **6**, 392-412.
55. J. Korang, I. Emahi, W. R. Grither, S. M. Baumann, D. A. Baum, R. D McCulla, *RSC Adv.,* 2013, **3**, 12390-12397.

Table of content entry

Car-Parrinello MD simulations and advanced visualization techniques of OH*-pair encounters in water demonstrate the formation of the triplet oxygen atom.